Applied Catalysis B: Environmental 179 (2015) 344–351

Contents lists available at ScienceDirect

Applied Catalysis B: Environmental

journal homepage: www.elsevier.com/locate/apcatb

Investigation of nitrogen doped and carbon species decorated TiO_2 with enhanced visible light photocatalytic activity by using chitosan

Yu Shao, Changsheng Cao, Shiliang Chen, Miao He, Jialin Fang, Jing Chen, Xiaofang Li, Danzhen Li*

Research Institute of Photocatalysis, State Key Laboratory of Photocatalysis on Energy and Environment, Fuzhou University, Fuzhou 350002, PR China

ARTICLE INFO

Article history:
Received 18 March 2015
Received in revised form 6 May 2015
Accepted 11 May 2015
Available online 14 May 2015

Keywords:
TiO_2
Chitosan
Nitrogen doped
Carbon species decorated
Photocatalytic degradation

ABSTRACT

Nitrogen-doped and carbon species decorated TiO_2 composites (Cts/TiO_2) are prepared by using chitosan as a natural nitrogen and carbon source to combine with TiO_2 by a facile and low-cost method for the first time. Their structures and properties are characterized by X-ray diffraction (XRD), UV–vis diffuse reflectance spectroscopy (DRS), Fourier-transform infrared spectroscopy (FT-IR), X-ray photoelectron spectroscopy (XPS), N_2 adsorption–desorption isotherms (BET), and electron spin resonance spectroscopy (ESR). The results show that the visible light absorption range of the composites even can be extended to 650 nm. Photocatalytic degradation of Rhodamine B (RhB) under visible light (420 nm < λ < 800 nm) irradiation is used as a model reaction to evaluate the photocatalytic activity of the composites. When the additive amount of chitosan is 0.25 g, the sample Cts/TiO_2-25 possesses the highest activity, which is over 4.8 times of N-TiO_2. The detection of active species during the photocatalytic process shows that superoxide radicals ($O_2^{\bullet -}$) play the most important role, then the probable degradation mechanism of the photocatalysts is proposed simultaneously. It is hoped that our work will open a new doorway to use a simple and green method to get high-efficiency TiO_2-based photocatalysts.

1. Introduction

Heterogeneous photocatalysis is an efficient method toward environmental remediation [1–4]. Due to its superior photocatalytic performance, high chemical stability, low cost, and environmental friendliness, titanium dioxide (TiO_2) is considered as an outstanding photocatalyst. However, the wide band gap of TiO_2 (3.2 eV for anatase) makes it only absorb UV light with the wavelength less than 387 nm, which is not more than 5% in solar spectrum. Thus, the visible light which accounts for most of the solar spectrum cannot be used. For the sake of expanding the optical response of TiO_2 to the visible light region, various efforts have been explored, such as surface sensitization by using dyes or carbon materials, doping with metal or non-metal elements, depositing with noble metals and preparing composite semiconductors [5–10]. Doping is thought as the most common and accessible method in deed. Metal elements like Fe, Co, Ni, Mn or V as dopants can efficiently improve the visible light photocatalytic activity of TiO_2 [11–15]. However, the low thermal stability and the increased electron-hole recombination sites by the dopants hinder its further development [16]. In fact, non-metal doping is thought more effective than metal doping. N, F, C, S, or I doped TiO_2 have been all proved as highly efficient photocatalysts with a visible light response [10,17–20]. However, S doping can lead to the poison of the catalysts easily [21], C doping usually need a severe high temperature [22], F anion is thought highly toxic to human and environment. Therefore, N doping may be a considerable choice.

Since the pioneering discovery by Asahi et al. [10], masses of works of N-doped TiO_2 have appeared. Various synthesis methods have been reported, such as direct amination of TiO_2 by using triethylamine as nitrogen source [23], solvothermal approach by using guanidine carbonate or diethylenetriamine as N dopant source [24,25], using urea as N source in a sol-gel process [26] and treating the TiO_2 precursor in triethylamine/ethanol fluid under supercritical conditions [27]. At the same time, the origin of the visible light photocatalytic activity of N-doped TiO_2 and the influence of N dopant concentration on the photocatalytic activity are studied [28,29]. However, some problems of N doping are still need to be solved urgently: first, it is difficult to prepare N-doped TiO_2 with high N dopant concentration; second, when the lattice O atoms are replaced by N atoms, oxygen vacancies [30] or Ti^{3+} [31] defaults will be introduced inevitably. Those defaults may become the recombination centers of the photo-generated carriers, resulting in the decreased photocatalytic activity; third, the stability of N-doped

* Corresponding author Tel.: +86 591 83779256; fax: +86 591 83779256.
E-mail address: dzli@fzu.edu.cn (D. Li).

http://dx.doi.org/10.1016/j.apcatb.2015.05.023
0926-3373/

TiO_2 during photocatalytic process is poor under visible light irradiation due to the decrease of N dopant concentration.

Furthermore, it is reported that the visible light photocatalytic activity and stability of TiO_2 can be improved by decoration with some carbon materials (i.e. graphene, mesoporous carbon, carbon quantum dot etc.) [32–35]. Carbon materials in the semiconductor composites can act as trapping centers for photo-induced electrons. The strong interactions between carbon materials and TiO_2 will promote the transmission and separation of photo-generated carriers. Furthermore, carbon materials can also serve as sensitizers to sensitize TiO_2 under visible light irradiation. As a result, the visible light photocatalytic activity of TiO_2 can be improved [6].

Therefore, it may be feasible to decorate N-doped TiO_2 with carbon materials to improve the photocatalytic activity and stability of N-doped TiO_2. Wang et al. use lysine as nitrogen and carbon source to prepare N-doped and carbon decorated TiO_2 with superior performance for the photocatalytic degradation of methyl orange (MO) under visible light irradiation [36]. Liu and Chen prepared activated carbon (AC) supported N-doped TiO_2 ($TiO_{2-x}N_y$/AC) by heating TiO_2 precursor/AC in a NH_3/N_2 atmosphere, showing excellent phenol degradation performance under visible light irradiation [37]. However, the improvement of stability of N-TiO_2 is limited. After several cycles, the deactivation of the catalysts still happens.

Unlike most of using inorganic or small organic molecules as the nitrogen and carbon source, using natural polymer (e.g. chitosan) as the nitrogen and carbon source is unreported. Chitosan (Cts), a kind of polysaccharide derivatives, is fully or partially derived from deacetylation of chitin. The presence of the large numbers of reactive hydroxyl and amino groups in its molecules can provide the sites for numerous chemical reactions on the surface of TiO_2 [38].

Herein, the TiO_2-based composites (Cts/TiO_2) with N-doping and carbon species decorating in the presence of chitosan are prepared by a two-step process for the first time. Compared with N-TiO_2 and the as-prepared TiO_2, the Cts/TiO_2 composites show much improved photocatalytic activity and stability for photocatalytic degradation of Rhodamine B (RhB) under visible light (420 nm < λ < 800 nm) irradiation. We hope our work can provide a green and low consumption way to get TiO_2-based photocatalysts with high-efficiency activity under visible light irradiation.

2. Experimental

2.1. Materials

Acetic acid (HAc) and isopropyl alcohol (IPA) were analytical grade, purchased from the Shanghai Chemical Co. Titanium (IV) isopropoxide (TIP), chitosan (degree of deacetylation ≥95%) were bought from Aladdin Reagent. Commercial anatase TiO_2 was purchased from Sigma–Aldrich. All of the chemicals were used without any further purification in the experiments. Deionized water was used for all experiments.

2.2. Preparation of the samples

Scheme 1 illustrates the preparation procedure of Cts/TiO_2 composites. First, 0.25 g Cts, 8 mL HAc, 12 mL H_2O and 20 mL IPA were mixed together to form solution (A). Then, 5 mL TIP, 22 mL IPA and 8 mL HAc were mixed to form solution (B). Next, solution (B) was added dropwise to solution (A) with continuous stirring. After several minutes of stirring at room temperature, the mixture was transferred into a Teflon-lined stainless steel autoclave. The autoclave was kept at 80 °C for 12 h in an electric oven. After the autoclave was naturally cooled to ambient temperature, the precipitation was centrifuged and washed with deionized water and absolute ethanol for several times and then dried at 60 °C in an electric oven. Finally, the precipitation was calcined at 300 °C for 4 h in a muffle furnace. This sample was designated as Cts/TiO_2-25. Varying the additive amount of Cts from 0, 0.1, 0.2, and 0.3 g in the preparation process, other samples were designated as TiO_2, Cts/TiO_2-10, Cts/TiO_2-20 and Cts/TiO_2-30, respectively. As a reference, N-doped TiO_2 (N-TiO_2) was prepared by annealing commercial anatase TiO_2 powders under NH_3 stream at 550 °C for 3 h [39].

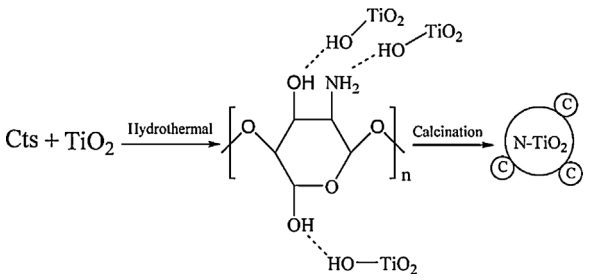

Scheme 1. Mechanism diagram of the formation of the catalyst during the preparation process.

2.3. Characterization of samples

The X-Ray diffraction (XRD) patterns were measured by a PA Nalytical X'Pert spectrometer with Co Kα radiation (λ = 1.78897 Å), then, the data were changed to Cu Kα data, to identify the phase constitutions in samples [40]. The morphology and particle size of the samples were recorded by transmission electron microscopy (TEM) images, which were obtained by using a FEI Tecnai G2 F20 instrument operated at an accelerating voltage of 200 kV. The diffuse reflectance spectra (DRS) of the composites were performed on a Varian Cary 500 UV–vis spectrophotometer with $BaSO_4$ as the background ranging from 200 to 800 nm. The flat band potential (V_{fb}) of Cts/TiO_2-25 was determined by the electrochemical method, which was measured on a PAR VMP3 Multi Potentiostat apparatus with a three-electrode cells. The catalyst was deposited on a 0.5 cm × 0.5 cm ITO glass to act as the working electrode, Ag/AgCl electrode as the reference electrode, and Pt as the counter electrode. The electrolyte was 0.1 mol/L Na_2SO_4 solution. The Mott–Schottky plots were obtained at three different frequencies (0.5 k, 1 k and 1.5 k Hz). The total organic carbon (TOC) assays of the reaction solution were carried out on a Shimadzu TOC-VCPH total organic carbon analyzer. The generated intermediates of RhB during photocatalytic process were analyzed by a gas chromatography-mass spectroscopy (GC–MS, Agilent 7890B for gas chromatography and Agilent 5977A for mass spectroscopy) with a column of HP-5 (30 m × 0.25 mm). The pretreatment process of sample was as follows: 5 mL reaction solution was extracted with 10 mL ethyl acetate for three times. Afterward, the extracted solution was dried by distilling under reduced pressures. Then the residues were dissolved in ethyl acetate. X-ray photoelectron spectroscopy (XPS) analysis was measured on a ESCALAB 250 photoelectron spectroscopy (Thermo Fisher Scientific Inc.) at 3.0×10^{-10} mbar with monochromatic Al Kα radiation (E = 1486.2 eV). To determine the amount of carbon species in the samples, thermogravimetric analysis (TGA) was performed using a CHNS/O analyzer (PE 2400II, Perkin Elmer, America) under nitrogen atmosphere, with a heating rate of 10 °C/min from ambient temperature to 800 °C. Fourier-transform Infrared Spectroscopy (FT-IR) analyses were conducted on a Nicolet Avatar 670 FI-IR spectrometer (Nicolet Corp., USA). Absorption bands were observed from 4000 to 400 cm^{-1} with 32 samples scans and 4.0 cm^{-1} resolution. The Raman spectra were recorded in a Renishaw inVia Raman microscope with a 785 nm laser. The Brunauer–Emmett–Teller (BET)

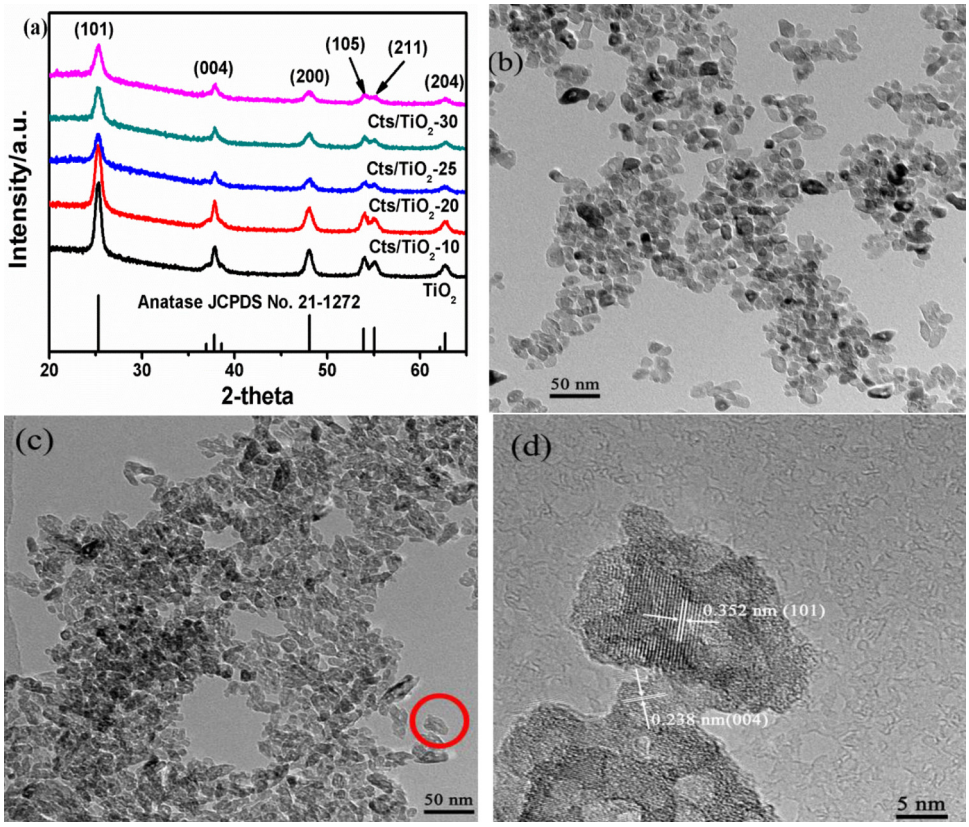

Fig. 1. (a) XRD patterns of the as-prepared catalysts; TEM images of (b) the as-prepared TiO_2; (c) Cts/TiO_2-25; (d) HRTEM image of Cts/TiO_2-25 (image (d) is the amplification of the marked location of image (c) with red circle).(For interpretation of the references to colour in this figure legend, the reader is referred to the web version of this article.)

specific surface area of the composites were analyzed by nitrogen adsorption at 77 K on an Autosorb-1C-TCD physical adsorption instrument (American Quantach-rome) using a Micrometrics ASAP 2020 system. The Electron spin resonance (ESR) spectra were obtained by a Bruker model A300 spectrometer to detect the generation of activated species under visible light irradiation (420 nm < λ < 800 nm). The settings of the ESR spectrometer were as followed: center field, 3512 G; microwave frequency, 9.86 GHz; microwave power, 20 mW. The generation of hydroxyl radicals was measured by the method of photoluminescence technique with terephthalic acid (PL-TA) [41]. The photoluminescence spectra were recorded by Edinburgh FL/FS900 spectrometer. The intensity of the peak at 426 nm is proportion to the amount of •OH radicals. The excitation light employed in recording fluorescence spectra was 312 nm. The detection of hydrogen peroxide (H_2O_2) was conducted by a photometric method in which N,N-diethyl-*p*-phenylenediamine (DPD) is oxidized by peroxidase (POD) and H_2O_2 [42]. The intensity of the absorption peaks at 510 nm and 551 nm is proportion to the amount of H_2O_2.

2.4. Tests of photocatalytic activity

Degradation of Rhodamine B (RhB) (1×10^{-5} mol/L) was used as the model reaction to evaluate the photocatalytic activity. A 500 W Xe-arc lamp (Institute of Electric Light Source, Beijing) was used as the light source, which equipped with 420 and 800 nm cutoff filters to ensure that reaction was subjected by visible light. The photocatalytic reaction was processing in a 100 mL Pyrex glass vessel, and 80 mg catalysts were added into 80 mL of RhB solution. Before irradiation, the suspensions were magnetically stirred in dark for 1 h to establish the adsorption–desorption equilibrium between catalysts and solution. During the irradiation, 3 mL aliquots were sampled in a certain time interval, and then centrifuged to remove the catalysts. Finally, the supernatants were analyzed by a Varian UV–vis spectrophotometer (Carry-50, Varian Co.) The photocatalytic conversion ratio is recognized as C/C_0, where, C_0 is the adsorption equilibrium concentration of solution, C is the concentration of solution at time t. And the concentration of RhB solution is monitored by the intensity of the absorption peak at 554 nm.

3. Results and discussion

Fig. 1(a) shows the XRD patterns of the as-prepared TiO_2 and the Cts/TiO_2 composites. It shows that all diffraction peaks can be fully indexed to standard peaks of anatase crystalline phase of TiO_2 (JCPDS 21-1272), which indicates the addition of chitosan could not impact the lattice structure of TiO_2. It can also be proved by matching the interplanar spacing d = 0.352 nm and 0.238 nm of Cts/TiO_2-25 with the (1 0 1) and (0 0 4) crystallographic plane of anatase TiO_2. With the amount of chitosan increasing, the decrease in the intensity and sharpness of the diffraction peaks indicates the decreased crystallinity and particle size of the composites. Fig. 1(b) and (c) are the TEM image of Cts/TiO_2-25 and the as-prepared TiO_2. It confirms that these samples are both composed by a mass of irregular nanoparticles, which means that the addition of chitosan cannot change the morphologies of TiO_2 nanoparticles obviously. The average size of Cts/TiO_2-25 nanoparticle calculated from the Scherrer formula is about 12 nm, which is corresponding to the result reading from the HRTEM images (Fig. 1(d)).

UV–vis diffuse reflectance spectra are used to evaluate the light absorption and band gap of the catalysts. It is clearly shown in Fig. 2(a) that the as-prepared TiO_2 mainly absorbs UV light, while the composites can absorb both UV and visible light. With the amount of Cts increasing, the light absorption of the composites

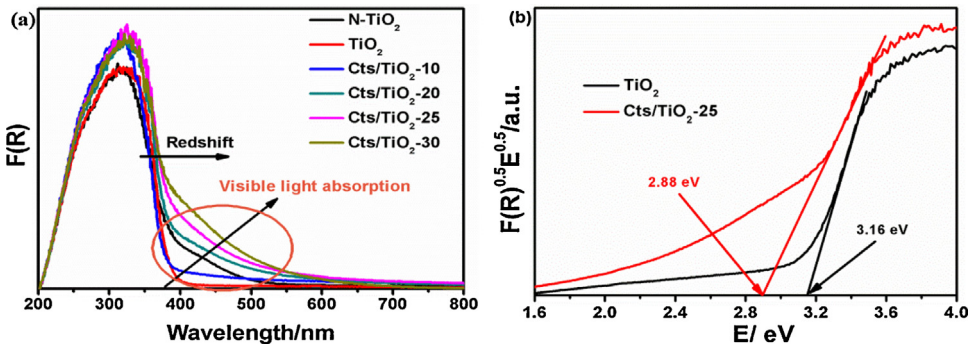

Fig. 2. (a) UV–vis diffuses reflectance spectra of the as-prepared catalysts; (b) Band gap energy (E_g) of the as-prepared TiO_2 and Cts/TiO_2-25.

Table 1
BET specific surface area of the as-prepared catalysts.

BET $m^2\ g^{-1}$	129.49	144.47	163.20	189.09	160.61
	TiO_2	Cts/TiO_2-10	Cts/TiO_2-20	Cts/TiO_2-25	Cts/TiO_2-30

is enhanced. The enhanced parts shown in Fig. S1 illustrate that the visible light absorption threshold of the composites can be extended to as much as 650 nm. Fig. 2(b) shows the band gap energy (E_g) of the as-prepared TiO_2 and Cts/TiO_2-25, which is calculated by the equation of $(F(R)E)^{1/2} = A(E-E_g)$ [43]. The estimated E_g values of the as-prepared TiO_2 and Cts/TiO_2-25 are 3.16 eV and 2.88 eV, respectively. Combined with the result of Mott–Schottky curves (Fig. S2), the conduction band and valence band values of Cts/TiO_2-25 are −0.53 eV and 2.33 eV, respectively.

Table 1 shows the BET specific surface area of the as-prepared TiO_2 and the Cts/TiO_2 composites. Compared with the as-prepared samples, the Cts/TiO_2-25 has the largest BET specific surface area values (189.09 $m^2\ g^{-1}$). Larger surface area may lead to the better photocatalytic activity.

The photocatalytic activities of the composites are evaluated by the degradation of RhB solution at ambient temperature. For comparison, the photocatalytic activities of N-TiO_2 and the as-prepared TiO_2 are conducted by the same condition, and the process without photocatalyst is labeled as blank. It is clearly seen in Fig. 3 that the Cts/TiO_2 composites display higher phtocatalytic activity. Among the samples, Cts/TiO_2-25 shows the best performance. After 30 min irradiation, the conversion ratio of RhB can reach to 96.8%, while the values of blank, N-TiO_2, as-prepared TiO_2, Cts/TiO_2-10, Cts/TiO_2-20 and Cts/TiO_2-30 are 1.7%, 19.9%, 38.2%, 65.4%, 87.5% and 90.3%, respectively. Fig. S3 shows the temporary absorption spectral changes of RhB by Cts/TiO_2-25 during the photocatalytic degradation process. The maximal absorption peaks show a blue-shift and broaden simultaneously with time going, which is originated from the de-ethylation process of RhB [44,45]. The de-ethylation efficiency is expressed by the shift rate of the maximal absorption peaks, which is also a way to evaluate the degradation efficiency of RhB by photocatalysts. It shows similar phenomena of the de-ethylation process for other Cts/TiO_2 composites. Fig. S4 displays the maximal absorption peak shift rate of the composites. The order of the shift rate is consistent with the order of the photocatalytic activity of the samples, and the Cts/TiO_2-25 also shows the maximum shift rate. Furthermore, the de-ethylation process is almost completed in 30 min after irradiation. Moreover, it is different with the conversion ratio of RhB, and the mineralization efficiency of RhB measured by TOC is also used to evalute the photocatalytic performance of photocatalytsts. It is clearly shown in Fig. S5 that nearly 50% TOC was removed in the presence of Cts/TiO_2-25, which is far exceeds than that of the as-prepared TiO_2 and N-TiO_2. On the other hand, because not all of TOC was removed, it means that RhB molecules are not totally mineralized. Therefore, some intermediates of RhB should be generated during the photocatalytic degradation process. Results in Fig. S6 show that some aromatic compounds are detected. Combined with the result of TOC and GC-MS, the possible photocatalytic degradation pathways of RhB over Cts/TiO_2-25 are shown in Fig. S7.

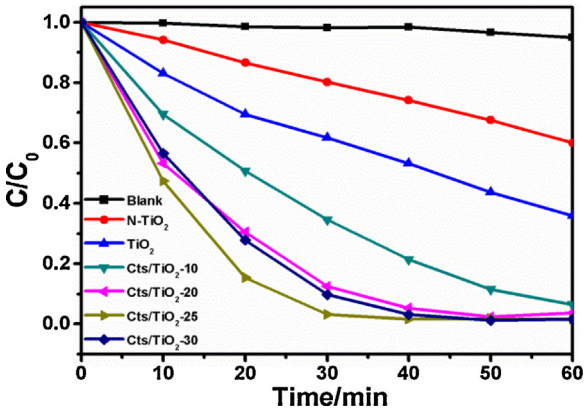

Fig. 3. Photocatalytic degradation of RhB over the as-prepared catalysts under visible light irradiation (420 nm < λ < 800 nm).

In order to exclude the photosensitization effect during the photocatalytic process by the as-prepared TiO_2 and the Cts/TiO_2 composites. Additional experiments are conducted: similar to the photocatalytic activity tests of the as-prepared photocatalysts, a high concentration of RhB solution as a liquid filter is placed between the light source and the glass vessel. The result is shown in Fig. 4(a), the visible light spectra excited the RhB molecules can be absorbed by the high concentration of RhB solution. Thus, the photodegradation of RhB is proceeding by photocatalytic process rather than photosensitization effect. It is shown in Fig. 4(b) and (c) that after add the high concentration RhB solution, the photocatalytic activity of the as-prepared TiO_2 decrease sharply, while it has little effect for Cts/TiO_2-25. Therefore, it can be concluded that the photodegradation of RhB by the as-prepared TiO_2 is driven by photosensitization effect. While for Cts/TiO_2-25, the degradation of RhB due to the photosensitization effect can be ignored, which further suggests that the activity over Cts/TiO_2-25 is attribute to the absorption of visible light.

Stability is an important factor of a catalyst. Cyclic photocatalytic degradation of RhB solution is conducted to detect the activity stability of Cts/TiO_2-25 and N-TiO_2. The results are shown in Fig. 5. After 5 cycles, the activity of N-TiO_2 decreases about 30%. When focusing on Cts/TiO_2-25, it has almost the same high-efficiency photocatalytic performance during the 5 cycles. The XRD patterns

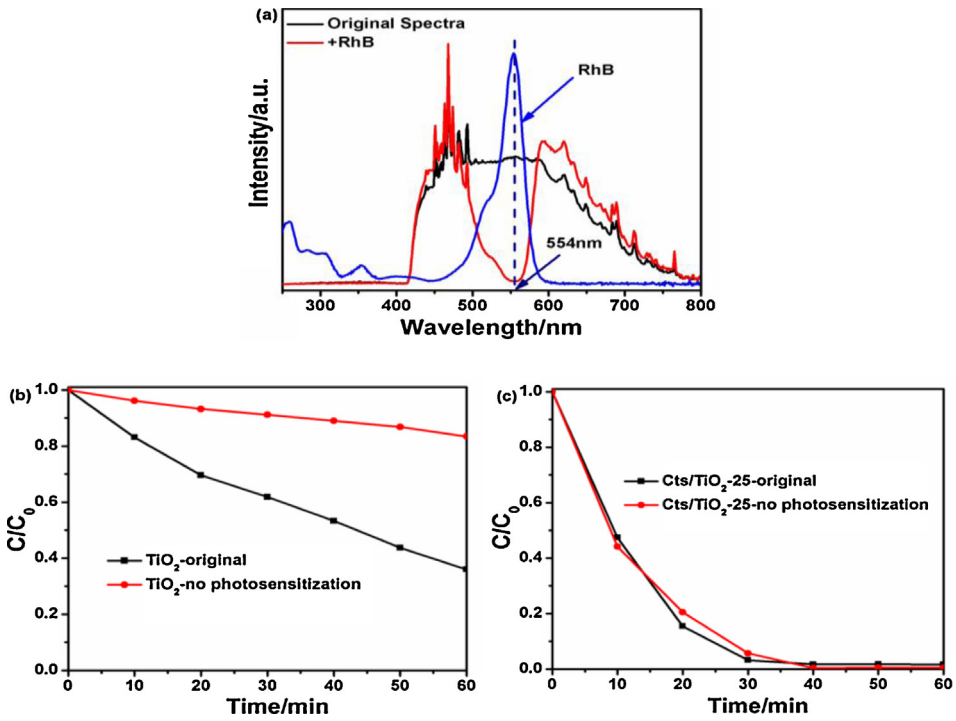

Fig. 4. (a) The light spectra before and after the addition of RhB; the results of photosensitization excluding experiments of (b) the as-prepared TiO_2 and (c) Cts/TiO_2-25.

of Cts/TiO_2-25 before and after the photocatalytic degradation of RhB are almost the same, indicating the best structural stability of the Cts/TiO_2 composites during the photocatalytic process (Fig. S8). Therefore, it is no doubt to say that during the photocatalytic process, Cts/TiO_2-25 has superior stability than N-TiO_2.

Fig. 6 shows the collected FT-IR spectra of the as-prepared TiO_2 and the Cts/TiO_2 composites. The peaks at 3411 cm^{-1} and 1633 cm^{-1} are attributed to the stretching vibration of H—O—H bond from the molecularly adsorbed H_2O, —OH or —COOH groups on the TiO_2 surface [46]. The peak at 662 cm^{-1} is attributed to the vibration of Ti—O—Ti [46]. Moreover, compared with the as-prepared TiO_2, another peaks appear at 1435 cm^{-1} and 1536 cm^{-1} on the composites' FT-IR spectra, which are corresponding to the vibration of —C—C— and —C═O groups [47]. Those results indicate that there exist many carbon-contain groups on the surface of Cts/TiO_2 composites, which will enhance the absorption of visible light. Besides those carbon-contain groups, carbon nanomaterials can also enhance the light absorption. The existence of carbon nanomaterials are proved in Cts/TiO_2-25 by Raman spectra (Fig. S9). However, the low contrast and poor crystallinity as compared to TiO_2 make it not exactly resolved in HRTEM image [48].

XPS survey spectra of the as-prepared TiO_2 and Cts/TiO_2-25 are shown in Fig. S10, and no obvious distinctions of the two samples are observed on the spectra. Thus, high resolution XPS spectra of C, N and Ti are further analyzed in Fig. 7. Three states of carbon species are evidenced by C 1s spectra in Fig. 7(a). No signal related to carbide (~282 eV) is observed, indicating that C doped into TiO_2 crystal is not happen [49]. The peak at binding energy (BE) of 284.6 eV is mainly attributed to the carbon tape and nonoxygenated carbon, and the peaks at BEs of 286.2 eV and 288.3 eV are assigned to —CO and —C═O groups [26,49,50]. However, the exact composition of the carbon-contain groups are still needed to be fully studied. Therefore, it can be confirmed that there exist carbon-contain groups and carbon materials on Cts/TiO_2-25 surface, which is correspond-

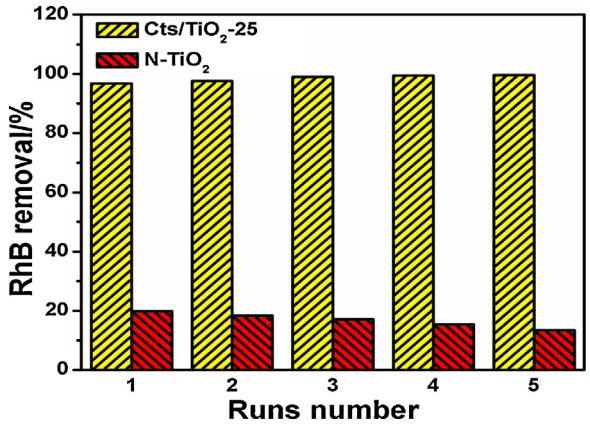

Fig. 5. Photodegradation stability of RhB over Cts/TiO_2-25 and N-TiO_2 under visible light irradiation (420 nm < λ < 800 nm) for 30 min.

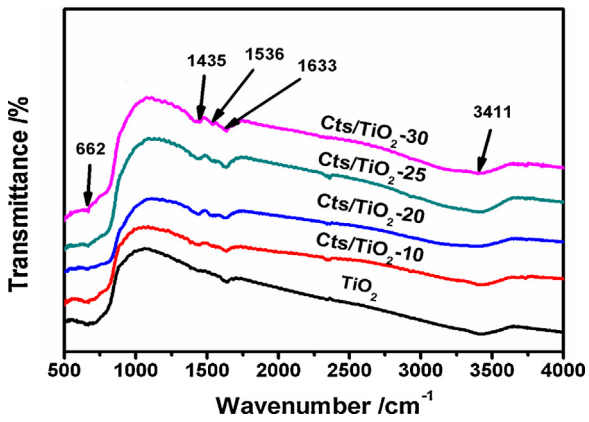

Fig. 6. FTIR spectra of the as-prepared catalysts.

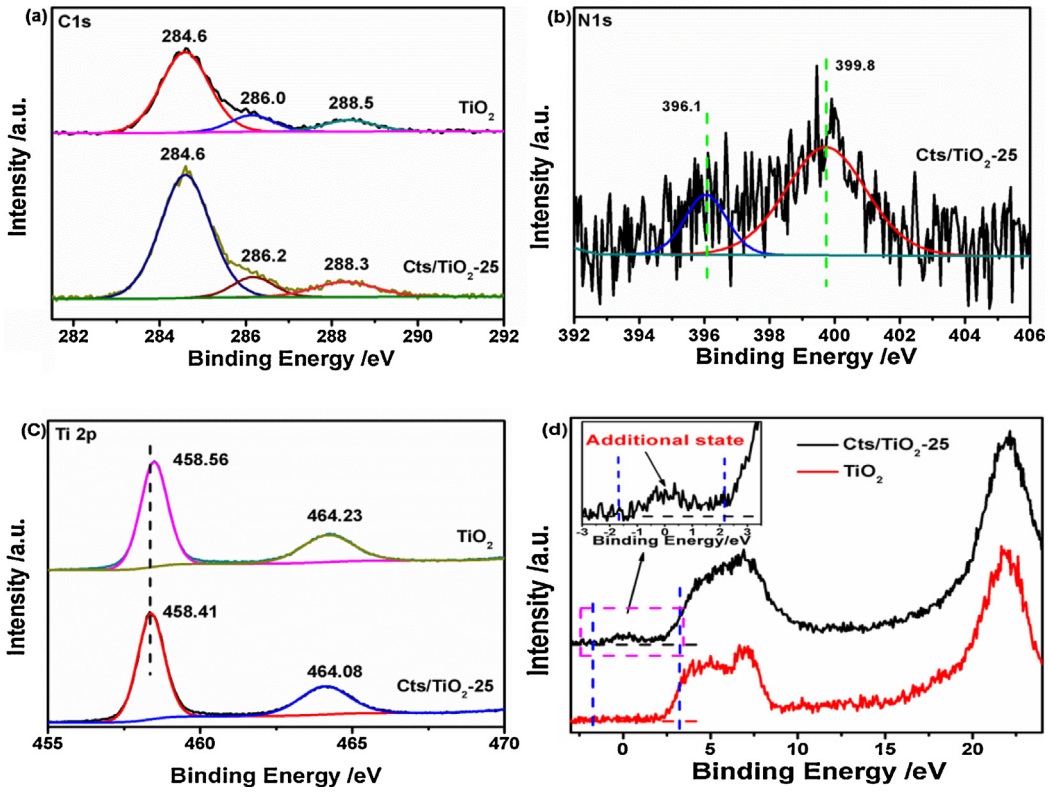

Fig. 7. XPS spectra of the as-prepared TiO_2 and Cts/TiO_2-25. (a): C 1s, (b): N 1s, (c): Ti 2p, (d): valence band (VB).

ing to the result of FT-IR and Raman spectra. From the analysis of TGA curves (Fig. S11), the content of those carbon-contain components in Cts/TiO_2-25 is 5.22%. Furthermore, there exist two peaks in the fitted curve of N1s XPS spectra of Cts/TiO_2-25 in Fig. 7(b). The peak at 396.1 eV is assigned to Ti-N-Ti bond, which illustrates that partial O atoms in TiO_2 are replaced by N atoms [10]. The other one at 399.8 eV is corresponding to the interstitial nitrogen-contain species [51]. Those results indicate that N has been doped into TiO_2 crystal successfully. From the XPS data, the amount of N dopant is counted ca. 0.48 at%. Based on the result of the N 1s and C 1s spectra (Fig. S12) before and after Ar etching for 60 s, it can help us deeply elucidate the doping situation of N and C atoms: the carbon-contain species really exist on the surface of Cts/TiO_2-25, rather than doped into the lattice of TiO_2, while the nitrogen-contain species should dope into the lattice of TiO_2.

Compared with the as-prepared TiO_2, the BE values of Ti 2p of Cts/TiO_2-25 have a 0.15 eV shift toward lower binding energy. This is due to the fact that the electronegative of N atom is smaller than of O atom. When partial O atoms are replaced by N atoms to generate Ti-N bonds, the electron density of Ti will increase. As a result, partial Ti^{4+} will be reduced to Ti^{3+}, thus, the BE of Ti 2p will decrease [36,52]. This further indicates the successfully doping of N atoms in Cts/TiO_2-25.

Fig. 7(d) shows the XPS spectra of valence band for the as-prepared TiO_2 and Cts/TiO_2-25. Compared with the as-prepared TiO_2, there appears an apparent additional electronic state above the valence band edge of Cts/TiO_2-25, indicating that there exists an additional band above the valence band [51,53], which results in visible light absorption. It is supposed that this additional band may originate from the carbon-contain groups and the N-doped species. Therefore, it can be concluded that the existence of the carbon-contain groups and the doped N species can lead to the visible light response of the composites. Furthermore, the carbon species (i.e. carbon materials and carbon-contain groups) in the composites will enhance the light absorption.

With the purpose of understanding the photocatalytic mechanism of pollutant degradation, ESR, TA-PL, H_2O_2, and scavenger detection experiments are conducted. It is known that the active species, such as e^-, h^+, $^{\bullet}OH$ radicals and $O_2^{\bullet-}$ radicals play important roles during the photocatalytic reaction process [54–56]. In order to detect the roles of those active species during the photocatalytic process, various active species scavengers are used. Fig. 8 shows the photocatalytic activities of Cts/TiO_2-25 toward the degradation of RhB under different conditions. As a kind of scavenger for $O_2^{\bullet-}$ radicals, the addition of 1 mg benzoquinone (BQ) can reduce the photocatalytic activity to the largest extent [57], indicating that $O_2^{\bullet-}$ radicals may play a very important role during the photodegradation process. Ammonium oxalate (AO) is used to trap holes [57]. After adding 0.1 g AO into the suspension, the pho-

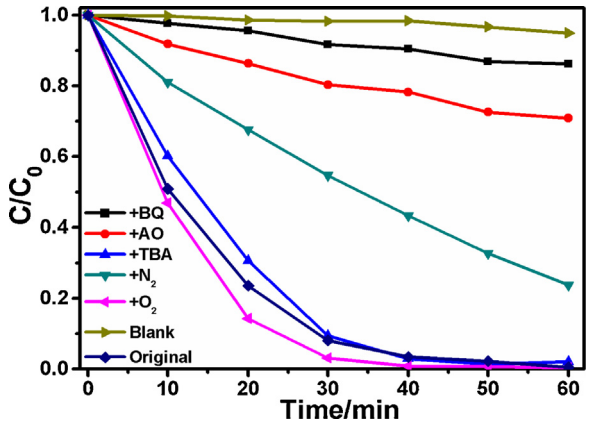

Fig. 8. Photocatalytic degradation of RhB over Cts/TiO_2-25 under different conditions with exposure to visible light (420 nm < λ < 800 nm).

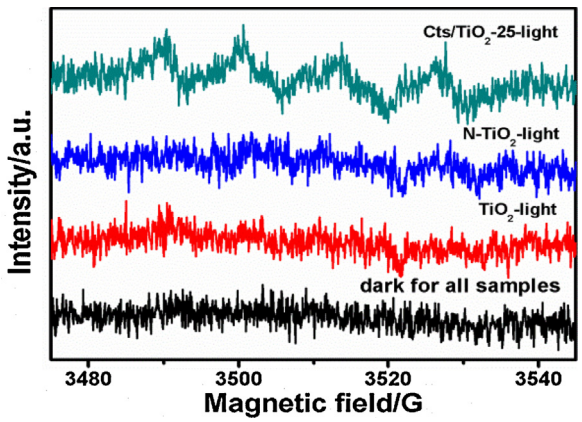

Fig. 9. DMPO spin-trapping ESR spectra of DMPO-$O_2^{\bullet-}$ for the as-prepared TiO_2, Cts/TiO_2-25 and N-TiO_2 under visible light (420 nm < λ < 800 nm) irradiation.

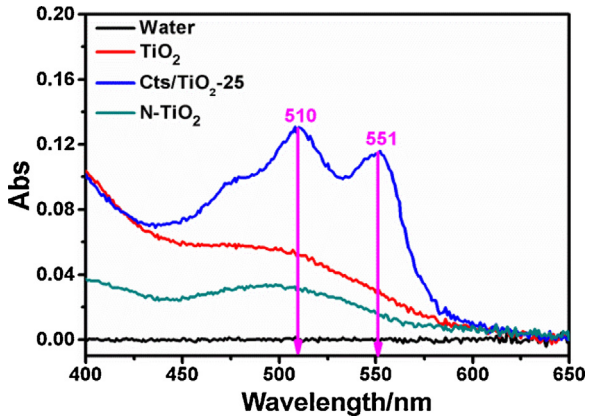

Fig. 10. Absorption spectra of the DPD/POD reagent after reaction with the as-prepared TiO_2, Cts/TiO_2-25 and N-TiO_2 under visible light (420 nm < λ < 800 nm) irradiation for 60 min.

todegradation degree of RhB decreased, which means holes also play an important role during the process. As an electron scavenger, O_2 can trap electrons to generate various kinds of active oxygen species. Therefore, the photocatalytic process will be prevented in anaerobic conditions. N_2 or O_2 bubbles through the suspension can be used to explore the impact of dissolved O_2 during the process. As a result, when bubbled with N_2, the activity reduces to some degree, while the activity increases a little when bubbled with O_2. Tert–butyl alcohol (TBA) is a kind of scavenger for •OH radicals. When adding 2 mL of TBA into the system, the activity only changed a little. On the other words, the photodegradation of RhB can be seldom driven by •OH radicals [57]. However, the result of the Mott–Schottky curves shows that •OH radicals cannot be generated by Cts/TiO_2-25. Therefore, it must exist other routes for Cts/TiO_2-25 to generate •OH radicals, reduction of H_2O_2 by electrons is a probable one [58]. According to the analysis of the above results, we conclude that the degradation of RhB is mainly achieved by $O_2^{\bullet-}$ radicals. Holes play a sub-mainly role, while •OH radicals contribute a less extent.

As a detection method, ESR spin-trapping technique with DMPO is used to further detect the •OH and $O_2^{\bullet-}$ radicals. As shown in Fig. 9, when irradiated with visible light, Cts/TiO_2-25 can generate stronger and more obvious peaks of DMPO-$O_2^{\bullet-}$ species than those of N-TiO_2 and the as-prepared TiO_2, indicating that Cts/TiO_2-25 can generate more $O_2^{\bullet-}$ radicals. Unfortunately, the signals of DMPO-OH• species cannot be observed clearly over the samples (data not shown). It may be due to the fact that the ESR technique is not the most suitable one to detect the •OH radicals in this system [59]. Therefore, TA-PL technique is taken to detect the generated amount of •OH radicals under visible light irradiation [60]. It is shown in Fig. S13 that the Cts/TiO_2 composites can generate a number of •OH radicals, which may come from the reduction of H_2O_2 by photogenerated electrons [58].

As an intermediate product during the photocatalytic process, H_2O_2 is not only as an important active species, but also can be reduced by electrons to generate •OH radicals. When adding DPD and POD into the suspension after 60 min of irradiation under visible light, the absorption peaks at 510 nm and 551 nm of Cts/TiO_2-25 suspension are obviously shown in Fig. 10 [42]. However, it does not appear obvious absorption peaks around 510 nm and 551 nm for the as-prepared TiO_2 and N-TiO_2 suspensions. The results above indicate that the Cts/TiO_2 composites can generate more H_2O_2 than those of the as-prepared TiO_2 and N-TiO_2, resulting in more •OH radicals.

Based on the results above, it can be concluded that Cts/TiO_2-25 can generate much more active radicals than other samples during the photocatalytic process, resulting in better photocatalytic activity. As a consequence, a probable degradation mechanism is proposed in the Scheme 2. Under visible light irradiation, photocatalytic degradation of dye over Cts/TiO_2 composites is proceed in the following way: The carbon-contain groups and the doped N species create an additional band above the valence band of TiO_2, which can be excited by visible light to generate carriers

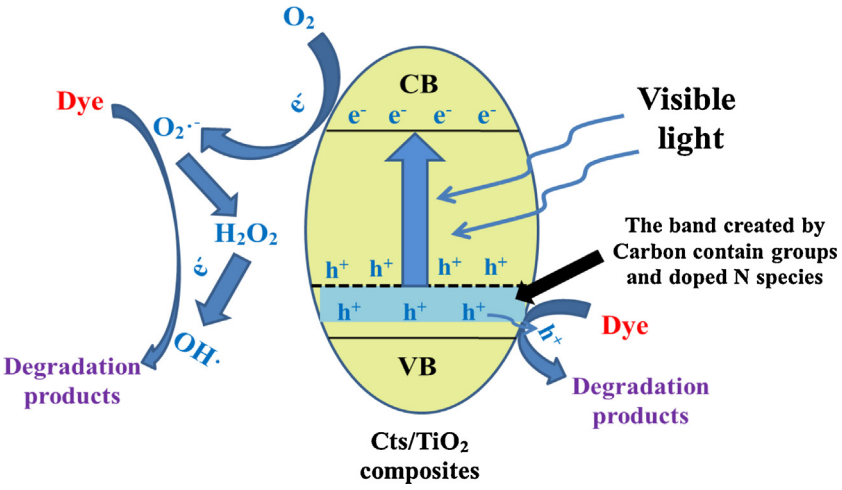

Scheme 2. Mechanism diagram of liquid-phase photocatalytic degradation of dye over Cts/TiO_2 composites under visible light irradiation.

(Eq. (1)). Next, the generated carriers take part in the generation of active species like $O_2^{\bullet-}$, $^{\bullet}OH$ radicals and H_2O_2 (Eqs. (2–4)). Finally, dye molecules are degraded by those active species (Eq. (5)).

$$Cts/TiO_2 + h\upsilon \rightarrow h^+ + e^- \quad (1)$$

$$O_2 + e^- \rightarrow O_2^{\bullet-} \quad (2)$$

$$O_2^{\bullet-} + 2H^+ \rightarrow H_2O_2 \quad (3)$$

$$H_2O_2 + e^- \rightarrow {}^{\bullet}OH + OH^- \quad (4)$$

$$h^+, O_2^{\bullet-}, H_2O_2, {}^{\bullet}OH \cdots + \text{Dye} \rightarrow \text{degradation products} \quad (5)$$

4. Conclusion

The Cts/TiO_2 nanocomposites are prepared by an improved hydrothermal-calcination process in the presence of chitosan for the first time. The crystalline phase of the composites is mainly of anatase, and the light absorption of composites can expand to visible light. Compared with the as-prepared TiO_2 and N-TiO_2, the Cts/TiO_2 composites show excellent photocatalytic performance in the degradation of RhB under visible light ($420\,nm < \lambda < 800\,nm$) irradiation. The enhanced photocatalytic activity may be attributed to the following reasons: first, the additional band above the valence band of TiO_2 is created by the carbon-contain groups and the doped N species, which can lead to the visible light response of the composites; second, the carbon species (i.e. carbon materials or carbon-contain groups) in the composites cannot only enhance the light absorption, but also enhance the stability of the composites; third, the large specific surface area of the Cts/TiO_2 composites is also benefit to photocatalytic activity. The results of active species detection show that the degradation of RhB process is mainly driven by $O_2^{\bullet-}$ radicals. Meanwhile, holes, H_2O_2 and $^{\bullet}OH$ also play important roles. Therefore, the Cts/TiO_2 composites have great potentialities to become photocatalysts with high activity and stability under visible light irradiation.

Acknowledgment

This work was financially supported by the National Natural Science Foundation of China (21173047 and 21373049).

Appendix A. Supplementary data

Supplementary data associated with this article can be found, in the online version, at http://dx.doi.org/10.1016/j.apcatb.2015.05.023

References

[1] C. Zhang, Y. Zhu, Chem. Mater. 17 (2005) 3537–3545.
[2] Y.-C. Zhu, Y. Bando, D.-F. Xue, D. Golberg, J. Am. Chem. Soc. 125 (2003) 16196–16197.
[3] A.L. Linsebigler, G. Lu, J.T. Yates, Chem. Rev. 95 (1995) 735–758.
[4] A. Fujishima, K. Honda, Nature 238 (1972) 37–38.
[5] A. Naldoni, M. Allieta, S. Santangelo, M. Marelli, F. Fabbri, S. Cappelli, C.L. Bianchi, R. Psaro, V. Dal Santo, J. Am. Chem. Soc. 134 (2012) 7600–7603.
[6] L. Zhao, X. Chen, X. Wang, Y. Zhang, W. Wei, Y. Sun, M. Antonietti, M.-M. Titirici, Adv. Mater. 22 (2010) 3317–3321.
[7] J. Yu, L. Qi, M. Jaroniec, J. Phys. Chem. C 114 (2010) 13118–13125.
[8] D. Kannaiyan, E. Kim, N. Won, K.W. Kim, Y.H. Jang, M.-A. Cha, D.Y. Ryu, S. Kim, D.H. Kim, J. Mater. Chem. 20 (2010) 677–682.
[9] D. Chatterjee, A. Mahata, Appl. Catal. B: Environ. 33 (2001) 119–125.
[10] R. Asahi, T. Morikawa, T. Ohwaki, K. Aoki, Y. Taga, Science 293 (2001) 269–271.
[11] B. Liu, H.M. Chen, C. Liu, S.C. Andrews, C. Hahn, P. Yang, J. Am. Chem. Soc. 135 (2013) 9995–9998.
[12] Z. Yao, F. Jia, S. Tian, C. Li, Z. Jiang, X. Bai, Acs Appl, Mater. Interfaces 2 (2010) 2617–2622.
[13] L. Pan, J.-J. Zou, X. Zhang, L. Wang, Ind. Eng. Chem. Res. 49 (2010) 8526–8531.
[14] J. Zhou, Y. Zhang, X.S. Zhao, A.K. Ray, Ind. Eng. Chem. Res. 45 (2006) 3503–3511.
[15] M. Shang-Di, L.B. Lin, D.L. Lin, J. Phys. Chem. Solids 55 (1994) 1309–1313.
[16] K. Pathakoti, S. Morrow, C. Han, M. Pelaez, X. He, D.D. Dionysiou, H.-M. Hwang, Environ. Sci. Technol. 47 (2013) 9988–9996.
[17] C. Han, M. Pelaez, V. Likodimos, A.G. Kontos, P. Falaras, K. O'Shea, D.D. Dionysiou, Appl. Catal. B: Environ. 107 (2011) 77–87.
[18] F. Dong, S. Guo, H. Wang, X. Li, Z. Wu, J. Phys. Chem. C 115 (2011) 13285–13292.
[19] W. Su, Y. Zhang, Z. Li, L. Wu, X. Wang, J. Li, X. Fu, Langmuir 24 (2008) 3422–3428.
[20] J.C. Yu, Yu, Ho, Jiang, Zhang, Chem. Mater. 14 (2002) 3808–3816.
[21] T. Umebayashi, T. Yamaki, H. Itoh, K. Asai, Appl. Phys. Lett. 81 (2002) 454–456.
[22] M. Janus, B. Tryba, M. Inagaki, A.W. Morawski, Appl. Catal. B: Environ. 52 (2004) 61–67.
[23] C. Burda, Y. Lou, X. Chen, A.C.S. Samia, J. Stout, J.L. Gole, Nano Lett. 3 (2003) 1049–1051.
[24] N.S. Chaudhari, S.S. Warule, S.A. Dhanmane, M.V. Kulkarni, M. Valant, B.B. Kale, Nanoscale 5 (2013) 9383–9390.
[25] J.H. Pan, G. Han, R. Zhou, X.S. Zhao, Chem. Commun. 47 (2011) 6942–6944.
[26] D. Chen, Z. Jiang, J. Geng, Q. Wang, D. Yang, Ind. Eng. Chem. Res. 46 (2007) 2741–2746.
[27] H. Yuning, J. Yi, Z. Jian, L. Hexing, Appl. Catal. B: Environ. 89 (2009) 543–550.
[28] Z. Zhang, Z. Luo, Z. Yang, S. Zhang, Y. Zhang, Y. Zhou, X. Wang, X. Fu, RSC Advances 3 (2013) 7215–7218.
[29] K. Yang, Y. Dai, B. Huang, J. Phys. Chem. C 111 (2007) 12086–12090.
[30] X. Pan, N. Zhang, X. Fu, Y.-J. Xu, Appl. Catal. A: Gen. 453 (2013) 181–187.
[31] G. Liu, J.A. Rodriguez, J. Hrbek, B.T. Long, D.A. Chen, J. Mol. Catal. A: Chem. 202 (2003) 215–227.
[32] X. Yu, J. Liu, Y. Yu, S. Zuo, B. Li, Carbon 68 (2014) 718–724.
[33] W. Wei, C. Yu, Q. Zhao, G. Li, Y. Wan, Chem. -Eur. J. 19 (2013) 796.
[34] K.-J. Chao, W.-Y. Cheng, T.-H. Yu, S.-Y. Lu, Carbon 62 (2013) 69–75.
[35] Y. Zhang, Z.-R. Tang, X. Fu, Y.-J. Xu, ACS Nano 5 (2011) 7426–7435.
[36] D.-H. Wang, L. Jia, X.-L. Wu, L.-Q. Lu, A.-W. Xu, Nanoscale 4 (2012) 576–584.
[37] S. Liu, X. Chen, J. Chem. Technol. Biotechnol. 82 (2007) 453–459.
[38] A. Watthanaphanit, P. Supaphol, T. Furuike, S. Tokura, H. Tamura, R. Rujiravanit, Biomacromolecules 10 (2009) 320–327.
[39] T. Tachikawa, Y. Takai, S. Tojo, M. Fujitsuka, H. Irie, K. Hashimoto, T. Majima, J. Phys. Chem. B 110 (2006) 13158–13165.
[40] Y. Liu, T. Lan, W. Zhang, X. Ding, M. Wei, J. Mater. Chem. A 2 (2014) 20133–20138.
[41] T.J. Mason, J.P. Lorimer, D.M. Bates, Y. Zhao, Ultrason. Sonochem. 1 (1994) S91–S95.
[42] H. Bader, V. Sturzenegger, J. Hoigné, Water Res. 22 (1988) 1109–1115.
[43] W. Li, D. Li, Z. Chen, H. Huang, M. Sun, Y. He, X. Fu, J. Phys. Chem. C 112 (2008) 14943–14947.
[44] W. Li, D. Li, S. Meng, W. Chen, X. Fu, Y. Shao, Environ. Sci. Technol. 45 (2011) 2987–2993.
[45] W. Zhao, C. Chen, X. Li, J. Zhao, H. Hidaka, N. Serpone, J. Phys. Chem. B 106 (2002) 5022–5028.
[46] P. Xu, J. Lu, T. Xu, S. Gao, B. Huang, Y. Dai, J. Phys. Chem. C 114 (2010) 9510–9517.
[47] X. Nie, G. Li, P.-K. Wong, H. Zhao, T. An, Catal. Today 230 (2014) 67–73.
[48] C. Lin, Y. Song, L. Cao, S. Chen, Nanoscale 5 (2013) 4986–4992.
[49] H. Wang, Z. Wu, Y. Liu, J. Phys. Chem. C 113 (2009) 13317–13324.
[50] J. Li, S. Tang, L. Lu, H.C. Zeng, J. Am. Chem. Soc. 129 (2007) 9401–9409.
[51] X. Chen, C. Burda, J. Am. Chem. Soc. 130 (2008) 5018–5019.
[52] M. Xing, J. Zhang, F. Chen, Appl. Catal. B: Environ. 89 (2009) 563–569.
[53] Y. Ma, X. Wang, Y. Jia, X. Chen, H. Han, C. Li, Chem. Rev. 114 (2014) 9987–10043.
[54] P. Wang, J. Xian, J. Chen, Y. He, J. Wang, W. Li, Y. Shao, D. Li, Appl. Catal. B: Environ. 144 (2014) 644–653.
[55] Y. Chen, D. Li, J. Chen, J. Wang, S. Meng, J. Xian, X. Fu, Y. Shao, Appl. Catal. B: Environ. 129 (2013) 403–408.
[56] D. Zhang, R. Qiu, L. Song, B. Eric, Y. Mo, X. Huang, J. Hazard. Mater. 163 (2009) 843–847.
[57] J. Wang, P. Wang, Y. Cao, J. Chen, W. Li, Y. Shao, Y. Zheng, D. Li, Appl. Catal. B: Environ. 136–137 (2013) 94–102.
[58] P. Salvador, J. Phys. Chem. C 111 (2007) 17038–17043.
[59] Y. Lin, D. Li, J. Hu, G. Xiao, J. Wang, W. Li, X. Fu, J. Phys. Chem. C 116 (2012) 5764–5772.
[60] S. Meng, D. Li, M. Sun, W. Li, J. Wang, J. Chen, X. Fu, G. Xiao, Catal. Commun. 12 (2011) 972–975.